ACS Catalysis

pubs.acs.org/acscatalysis Research Article

Activity Trends for the Selective Oxidation of 2-Propanol to Acetone on Noble Metal Electrodes in Alkaline Electrolyte

Iosif Mangoufis-Giasin,* Lukáš Fusek, Tian Yang, Peyman Khanipour, Olaf Brummel, Jörg Libuda, Karl J. J. Mayrhofer, Federico Calle-Vallejo,* and Ioannis Katsounaros*

Cite This: ACS Catal. 2023, 13, 14562−14569 Read Online

ACCESS | Metrics & More | Article Recommendations | Supporting Information

ABSTRACT: Fuel cells based on 2-propanol can be used to produce electricity utilizing the hydrogen stored in liquid organic hydrogen carriers. While the focus has previously been on acidic media, where only platinum-based electrodes are active, we explore here the oxidation of 2-propanol in alkaline solutions on different noble metal electrodes. Using experimental and computational methods, we find that the reaction is selective to acetone, whereas C−C bond breaking and the formation of adsorbed CO do not take place. The onset potential increases along the series Rh < Pt < Pd < Au, a trend that correlates with the adsorption energy of acetone on the respective surfaces. The oxidation rate decays under potentiostatic conditions due to the progressive accumulation of acetone at the surface. At high overpotentials, the reaction is limited by oxide formation. Given that alkaline systems are not restricted to exclusively platinum-based electrodes, a broader range of materials may be found that act as anodes for efficient 2-propanol fuel cells.

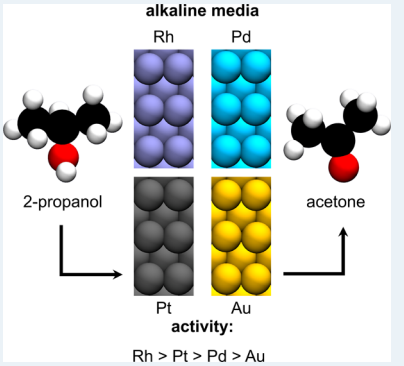

KEYWORDS: *hydrogen economy, liquid organic hydrogen carriers, alcohol fuel cells, isopropanol oxidation, fuel cell anodes, alkaline media, volcano plot, acetone adsorption energy*

1. INTRODUCTION

A major challenge for the implementation of a hydrogen-based economy is the transportation of hydrogen on a global scale. This issue can be addressed if hydrogen at the point of production (e.g., a water electrolyzer) is directly stored in hydrogen-carrying molecules, which can be distributed globally and release the hydrogen they contain at the point of use. Liquid organic hydrogen carriers (LOHCs) are attractive candidates for that purpose because, among other characteristics, they offer high volumetric energy density, are easy-to-handle liquids at ambient conditions, and are compatible with the existing infrastructure for fossil fuels.[1]

Previous work showed that a hydrogen-loaded LOHC (Hx-LOHC) can be utilized for electricity generation, if it is used to hydrogenate acetone via a catalytic transfer hydrogenation reaction (CTHR), and the formed 2-propanol is then oxidized in an isopropanol-fed polymer electrolyte membrane fuel cell (IPA-PEMFC) to deliver electricity.[2] The main advantage of IPA-PEMFCs over other alcohol fuel cells (e.g., based on methanol or ethanol) is that 2-propanol is oxidized selectively to acetone without the formation of CO_2, and the acetone formed at the anode can be recycled back and become again available for CTHR. Therefore, the integrated Hx-LOHC/IPA-PEMFC system can be operated in repetitive cycles with the supply of Hx-LOHC, which acts as the energy carrier, yielding H0-LOHC. The latter can be separately hydrogenated using, for example, hydrogen from electrolysis.

In acidic electrolytes resembling the conditions of a PEMFC, only platinum- and platinum-based electrodes are active for the oxidation of 2-propanol.[3] The selectivity to acetone stems from the difficulty to break the C−C bond of the secondary alcohol, thereby preventing the complete oxidation to CO_2.[4−7] This is additionally corroborated by in situ spectroscopic studies, which showed the absence of adsorbed CO during the oxidation of 2-propanol,[4,7,8] except for Pt(100) where a minor path to CO is viable.[9] Selective formation of the respective ketone is, in fact, a general characteristic of the oxidation of secondary alcohols such as 2-butanol, 2-pentanol, 3-pentanol, or 2,3-butanediol.[10,11] It should be emphasized that the above discussion is focused only at potentials that are relevant for fuel cell operation; bond cleavage and adsorbed CO as well as CO_2 formation may occur at higher potentials in the oxide region.

While platinum-based electrodes are also active in alkaline media,[12−17] a broader range of electrodes can oxidize 2-propanol compared to acidic media, such as gold,[14,17,18] rhodium,[19] palladium,[15−17,20] and palladium-based alloys.[21−23] Here, we study the electrooxidation of 2-propanol in alkaline

Received: July 25, 2023
Revised: September 27, 2023
Accepted: October 17, 2023
Published: October 30, 2023

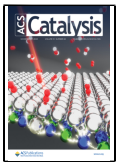

electrolytes on four noble metal electrodes aiming to establish the activity trends and rationalize them in terms of a simple activity descriptor. We use (a) electrochemical measurements to identify onset potentials and establish current−potential relationships, (b) vibrational spectroscopy and mass spectrometry to determine the reaction selectivity, and (c) computational modeling to elucidate the reaction pathways and justify trends in electrocatalytic activity for the four active metal surfaces. We find that the overpotential increases in the order Rh < Pt < Pd < Au, following the adsorption energy of acetone, which is the only detected product of the reaction in the studied potential range.

2. MATERIALS AND METHODS

2.1. Electrochemical Measurements. Standard electrochemical measurements (without product characterization) were performed in a classical three-electrode Teflon cell. All potentials in the manuscript are expressed with respect to the reversible hydrogen electrode (RHE), determined by measuring the open-circuit potential of a platinum wire versus the Ag/AgCl reference electrode in a hydrogen-saturated 0.1 mol L^{-1} NaOH solution (except for the spectroelectrochemical experiments, where a homemade RHE was used). Gamry Reference-600 potentiostats were used for all measurements. The electrolyte resistance was determined before each measurement with electrochemical impedance spectroscopy and compensation (by 90%) was performed using positive feedback; the remaining uncompensated resistance was always below 4 Ω. The spectroelectrochemical measurements were performed without resistance compensation. The electrolyte was prepared by dissolving NaOH pellets (EMSURE for analysis, Supelco) and 2-propanol (Merck Suprapure) in ultrapure water (Merck Millipore, resistance 18.2 MΩ·cm, total organic compounds - TOC < 5 ppb at 25 °C). All glassware and Teflon parts used in the electrochemical experiments were cleaned by storing them in sulfuric acid (98%, Merck) with NOCHROMIX (Sigma-Aldrich) for at least 12 h, rinsing, and subsequently boiling three times with ultrapure water. Furthermore, all metal wires were flame-annealed with a Bunsen burner and rinsed with ultrapure water.

2.2. Electrode Treatment. The working electrodes were polycrystalline Au, Pd, Pt, and Rh disks (5.0 mm diameter, 3.0 mm thickness, Mateck). All disks were polished using diamond paste with grain sizes of 0.25, 1, and 3 μm (Saint-Gobain Diamantwerkzeug GmbH). Afterward, they were sonicated in 3 steps with ultrapure water, 2-propanol, and ultrapure water (15 min each). Subsequently, electrochemical cleaning was performed for all disk electrodes. A first electrochemical cleaning step consisted of 100 cycles in 0.1 mol L^{-1} NaOH with a scan rate of 500 mV s^{-1} between 0 and 1.4 V_{RHE} (for Pt), 0.25 and 1.4 V_{RHE} (for Pd), 0.25 and 1.4 V_{RHE} (for Rh), and 0 and 2 V_{RHE} (for Au), followed by one chronoamperometry scan for 5 min at −0.1 V_{RHE} (for Pt), 0.2 V_{RHE} (for Pd), −0.1 V_{RHE} (for Rh), and −0.3 V_{RHE} (for Au). Although surface roughening is induced by this procedure, it was deemed essential to obtain reproducible voltammograms by removing adsorbates during the oxidation/reduction cycles and by reducing the surface during the potential hold step.

2.3. Electrochemical Real-Time Mass Spectrometry, EC-RTMS. Product analysis in real time by EC-RTMS was performed using a V-type flow cell coupled to direct analysis in real-time−time-of-flight mass spectrometer (DART-TOF-MS). The basic principles of EC-RTMS for the real-time characterization of electrolyte composition have been described in previous works.[24,25] In brief, a collection capillary was positioned close (ca. 100 μm) to the surface of the working electrode, and the electrolyte along with the reaction products was continuously withdrawn for analysis with DART-TOF-MS (JEOL JMS-T100LP AccuTOF). The dissolved acetone which formed after the oxidation of 2-propanol was analyzed in the negative mode, at the mass range m/z = 58.0−58.1 (ion structure $[^{13}C^{12}C_2H_6O - H]^-$). The counter electrode (Pt wire, Mateck GmbH) was placed at the waste channel of the V-type flow cell, i.e., separated from the collection capillary, to avoid any interference with the product analysis. The reference electrode was a Ag/AgCl in 3.0 mol L^{-1} KCl (BASi). The electrolyte, introduced continuously in the flow cell from an FEP canister, was purged with argon (Air Liquide, 4.8N) prior to each measurement for 20 min, and the gas flow was then maintained throughout the entire experiment.

2.4. Electrochemical Infrared Reflection Absorption Spectroscopy, EC-IRRAS. To identify the adsorbed intermediates and products during the electrooxidation of 2-propanol with high surface sensitivity, electrochemical infrared reflection absorption spectroscopy was used, known as EC-IRRAS. The counter electrode was a gold wire (Hauner, 99.999%), and the reference electrode was a home-built RHE. EC-IRRA spectra were measured using a Fourier transform infrared (FTIR) spectrometer with evacuated optics (Bruker Vertex 80v) and a liquid-nitrogen-cooled narrow-band mercury−cadmium-telluride (MCT) detector. The electrochemical cell consisted of a home-built Teflon housing with a CaF_2 hemispherical window (25 mm, Korth) sealed by a Kalrez gasket.[26] All spectra were recorded with a spectral resolution of 2 cm^{-1} and an acquisition time of 30 s (64 scans). For each measured potential, the electrode was cleaned by electrochemical cycling (see Section 2.2) in the retracted position. Subsequently, the thin layer was formed while holding the electrode at a constant potential of 0.0 V_{RHE} (for Pt, Rh, and Au) or +0.2 V_{RHE} (for Pd) for 3 min and reference spectra were measured afterward. IR spectra were measured at 0.6, 0.71, and 0.8 V_{RHE} for Pt; 0.6, 0.74, and 0.83 V_{RHE} for Pd; 0.145, 0.18, and 0.22 V_{RHE} for Rh; and 1.06, 1.16, and 1.22 V_{RHE} for Au both in p- and in s-polarization. The background of all IR spectra was corrected for better comparability by using the software OriginLab. All IR spectra are plotted as difference spectra with $\frac{\Delta R}{R} = \frac{\text{spectrum} - \text{reference}}{\text{reference}} \times 100\%$.

2.5. Computational Details. We used the Vienna Ab initio Simulation Package (VASP)[27] to carry out the DFT simulations with the Perdew−Burke−Ernzerhof (PBE) exchange-correlation functional,[28] the projector augmented-wave (PAW) method,[29] and a plane-wave cutoff of 450 eV. The choice of PBE to approximate the total DFT energies is justified in Section S4. To model Rh, Pd, Pt, and Au, two different surface models were used: (111) and (110) slabs. We used (2 × 2) supercell slabs containing four and seven atomic layers, respectively. The use of (2 × 2) cells is discussed in Section S4 in the light of lateral interactions between adsorbates, and a comparison is provided against (3 × 2) (110) cells. Converged PBE lattice constants of 3.84, 3.96, 3.98, and 4.18 Å were employed to build the surface models of Rh, Pd, Pt, and Au, respectively. The adsorbates and the top two/four layers of the (111)/(110) slabs were allowed to relax in all directions, while the remaining layers at the bottom were fixed at the bulk equilibrium distances. We smeared the Fermi level with the Methfessel-Paxton approach,[30] using k_BT = 0.2 eV, and the total energies were in all cases extrapolated to 0

https://doi.org/10.1021/acscatal.3c03423
ACS Catal. 2023, 13, 14562−14569

K. The numerical integration in the reciprocal space was carried out using Monkhorst−Pack[31] grids of 6 × 6 × 1/5 × 4 × 1 for (111)/(110) slab models, which ensured convergence of the adsorption energies within ±0.05 eV. The periodically repeated images were separated by more than 13 Å of vacuum in the z direction and dipole corrections were also applied. The conjugate gradient optimization algorithm was used for the atom relaxations with iterations performed until the maximum residual force on any atom was below 0.05 eV Å^{-1}. Boxes of 15.0 Å × 15.1 Å × 15.2 Å were used to calculate the free molecules (H_2, acetone, 2-propanol), considering only the Γ-point, k_BT = 0.001 eV and extrapolating the total energies to 0 K.

The free energies of reaction were evaluated using the formula: $\Delta G \approx \Delta E_{DFT} + \Delta ZPE - T\Delta S + \Delta E_{solv}$, where ΔE_{DFT} is the DFT-calculated reaction energy, ΔZPE is the zero-point energy change, $T\Delta S$ is the entropy change at 298.15 K, and ΔE_{solv} is a solvation correction for adsorbates calculated by means of an iterative microsolvation method[32,33] (see further details and specific values in Section S3). ΔS of free molecules were obtained from thermodynamic tables, while for adsorbates, ΔS only includes vibrational entropies. Vibrational frequency analyses were used to obtain the values of ZPE and S_{vib}, using the harmonic oscillator approximation. Gas-phase corrections (−0.08 and 0.05 eV for acetone and 2-propanol, respectively) were applied to ensure that the calculated equilibrium potential matches the experimental one.[34,35] The energies of 2-propanol and acetone in the liquid phase were approximated on the basis of those in the gas phase using a semiempirical method.[36] The computational hydrogen electrode was used to assess the energetics of proton−electron pairs.[37] The adsorption energies of all intermediates in this study are given in Section S3, and the direct coordinates of the most stable configuration of the adsorbed isopropoxide intermediate are also provided there.

3. RESULTS AND DISCUSSION

3.1. Linear Sweep Voltammetry. The positive-going linear sweep voltammograms (LSVs) for the electrooxidation of 2-propanol on four different polycrystalline disk electrodes (Au, Pt, Pd, and Rh) in an alkaline 0.1 mol L^{-1} NaOH electrolyte are shown in Figure 1. The lowest onset potential was observed for Rh (ca. + 0.1 V_{RHE}), which is close to the thermodynamic equilibrium potential for the acetone/2-propanol redox couple (+0.13 V at standard conditions, i.e., when thermodynamic activities for acetone and 2-propanol are unity).[2] The other electrodes activate 2-propanol at higher overpotentials, along the series Pt (ca. + 0.25 V_{RHE}) < Pd (ca. + 0.4 V_{RHE}) < Au (ca. + 0.8 V_{RHE}). For all electrodes, the oxidation current of 2-propanol reaches a maximum and then decreases until the reaction practically ceases at a potential where oxide formation takes place on the respective metal surface. In particular, when the 2-propanol oxidation voltammograms are compared with the ones in alkaline solution in the absence of 2-propanol (i.e., "blank" voltammograms", see Figure S1 in the SI), the suppression of the 2-propanol oxidation for all investigated electrodes coincides with the respective onset of surface oxidation. The maximum current density was recorded for Au (ca. 6.0 mA cm^{-2}), followed by Pd (ca. 4.0 mA cm^{-2}), whereas Pt and Rh exhibit the lowest peak current densities (both ca. 2.0 mA cm^{-2}).

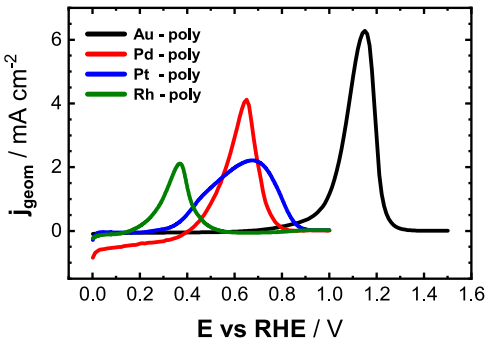

Figure 1. Electrooxidation of 2-propanol on Au, Pd, Pt, and Rh polycrystalline disk electrodes. Positive-going LSVs were in 0.1 mol L^{-1} NaOH and 0.2 mol L^{-1} 2-propanol. Scan rate: 5 mV s^{-1}.

If the performance of these electrodes in an alkaline electrolyte is compared with that in acid, it is remarkable that only platinum is active for 2-propanol oxidation in an acidic environment (see Figure S2 in the SI). Such a different behavior between acidic and alkaline solutions has been previously observed by Kwon et al. for gold[38] for a series of primary and secondary alcohols, and was attributed to the base-catalyzed deprotonation of the alcohol in solution, yielding an electroactive alkoxide ion (isopropoxide for 2-propanol). Recently, Mekazni et al.[39] showed that the oxidation of 2-propanol on platinum basal planes in acid, where isopropoxide ions are not present in solution, is facilitated by a reaction between *OH and isopropanol molecules, leading to the formation of the isopropoxide adsorbate, although the respective ions are not present in the electrolyte. Therefore, we propose that the ability of Pd, Rh, and Au to oxidize 2-propanol only in alkaline conditions is related to the abundance of bulk electroactive isopropoxide ions in solution. Note that, as will be shown later in the computational section, adsorbed isopropoxide is a key reaction intermediate.

3.2. EC-IRRAS Measurements. Electrochemical IR spectra were recorded for each disk electrode at three different potentials close to the potential with the highest activity (Pt: 0.6, 0.71, and 0.8 V_{RHE}, background at 0.0 V_{RHE}; Pd: 0.6, 0.74, and 0.83 V_{RHE}, background at 0.2 V_{RHE}; Rh: 0.145, 0.18, and 0.22 V_{RHE}, background at 0.0 V_{RHE}; Au: 1.06, 1.16, and 1.22 V_{RHE}, background at 0.0 V_{RHE}). The spectra with the highest band intensity are provided in Figure 2, and the complete data set is shown in Figure S3. At each potential, the spectra were measured in p- (sensitive to adsorbed species and species in solution) and in s-polarization (sensitive to species in solution only) without breaking the thin layer. This enabled us to compare directly the data measured with both polarizations. Note that all data are difference spectra ($\frac{\Delta R}{R} = \frac{[\text{spectrum} - \text{background}]}{\text{spectrum}}$) and negative bands (pointing downward) represent species formed at an applied potential, while positive bands (pointing upward) indicate consumed species.

All spectra consist of three sharp negative bands at 1700, 1370, and 1240 cm^{-1}, which we assign to the ν(C═O), $\delta_{sym}(CH_3)$/ν_{asym}(C−C), and ν_{asym}(C−C) of formed acetone, respectively.[40] Note that we observed identical bands for 2-propanol oxidation on platinum surfaces in acid.[8] At the same time, in all spectra, positive bands are visible at 1470, 1310, 1165, and 1130 cm^{-1}, which we assign to the $\delta_{sym}(CH_3)/\delta_{asym}(CH_3)$, δ(O−H), ν(C−C), and ν(C−O) of 2-propanol that is consumed.[8] Moreover, a broad band observable in the spectra between 1600 and 1700 cm^{-1} corresponds to water.[41]

Remarkably, no adsorbed carbon monoxide (CO_{ads}) is detected during the reaction on any of the studied surfaces or potentials applied, which would have been apparent by bands at

https://doi.org/10.1021/acscatal.3c03423
ACS Catal. 2023, 13, 14562−14569

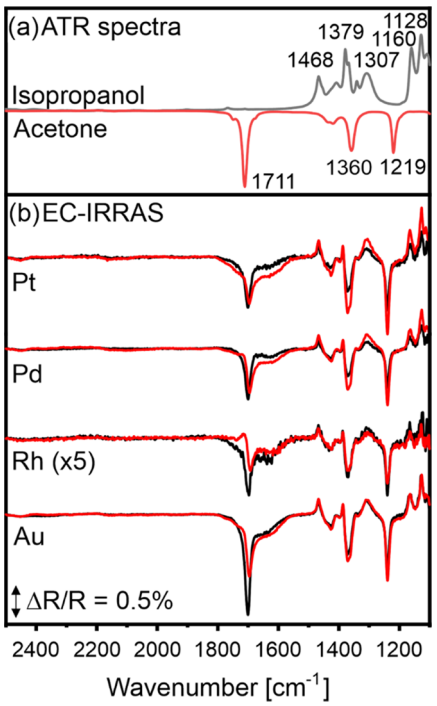

Figure 2. (a) ATR IR spectra of 2-propanol (black) and acetone (red). (b) EC-IRRAS spectra of 2-propanol oxidation recorded at a given electrode potential (Pt 0.8 V_{RHE}, Pd 0.83 V_{RHE}, Rh 0.22 V_{RHE}, Au 1.16 V_{RHE}) in *p*-polarization (black) and *s*-polarization (red). The intensity of Rh spectra was multiplied by 5. The reference of all spectra was measured at 0 V_{RHE} (for Pt), 0.2 V_{RHE} (for Pd), 0 V_{RHE} (for Rh), and 0 V_{RHE} (for Au). Note that all spectra are difference spectra, with positive bands indicating consumed species and negative bands indicating formed species.

ca. ~2040, ~1810, and ~1730 cm^{-1} for linearly, bridge, or 3-fold hollow bonded CO, respectively.[42] Given that EC-IRRAS in the *p*-polarization is highly sensitive to CO_{ads} (<1% of a monolayer), we can rule out that even traces of CO_{ads} are formed during the reaction.[43] The bands of carbonate (expected at 1366 and 1270 cm^{-1}) overlap with the bands of acetone and 2-propanol,[44] and consequently, the spectroelectrochemical experiments are not suitable to exclude the formation of traces of carbonate. Further, no CO_2 formation (expected at 2343 cm^{-1}) is observable, which would be a clear indication of a pH drop locally at the thin layer due to the H^+ formed during the electrooxidation reaction and a concomitant shift of the equilibrium among carbonate, bicarbonate, and carbonic acid toward the latter.[45] Apart from the aforementioned bands related to 2-propanol, acetone, and water, no other bands are observed in any of the spectra, regardless of the electrode used and the potential applied, indicating that acetone is formed on all surfaces with high selectivity. This reveals the difficulty in splitting the C−C bond of 2-propanol, which is a secondary alcohol, for any of the surfaces considered as also shown before for platinum electrodes in acid[7,8,10,46] or alkaline conditions.[16,47]

Comparing the spectra measured in *p*- and *s*-polarization, we find that all spectra show a higher intensity of the carbonyl band in *p*-polarization than in s-polarization. In addition, the intensity of the bands at 1700 cm^{-1}, as compared to the bands at 1370 or 1240 cm^{-1}, is higher in *p*-polarization than in s-polarization. Finally, all carbonyl bands show a slight shift of the band position in *p*-polarization. Altogether these observations indicate that part of the formed acetone remains adsorbed at the surface of all electrodes, which may lead to partial self-poisoning.[8] Taking into account the intensity ratio between the bands at 1700 cm^{-1} and those at 1240 and 1370 cm^{-1} in *p*- and *s*-polarization and the metal surface selection rule (MSSR), we conclude that acetone is weakly adsorbed on all surfaces, most likely in the η^1 configuration in which acetone binds with the oxygen to the surface. Such behavior was suggested previously on Pt(111) in acidic electrolytes.[8]

3.3. Product Analysis during Step Measurements. To investigate the evolution of 2-propanol electrooxidation over time at a constant potential, acetone was monitored in real time with EC-RTMS during chronoamperometric step measurements. The experimental protocol consisted of 5 min steps at a constant potential, which were separated by 5 min relaxation steps at 0 V_{RHE}. The potential at each successive electrolysis step was 50 mV more positive than the previous one. The relaxation step was necessary to regenerate the surface by removing adsorbed acetone as well as to ensure that the mass spectrometry signal for the formed acetone, I_{ACE}, reached the background level. For each electrode under study (Au, Pd, Pt, or Rh), the chronoamperometric experiment was designed to cover the potential range where 2-propanol is oxidized on the respective surface, as found from the LSVs.

The oxidation rate decays with time, regardless of the electrode used or the applied potential. This is apparent already from the current density versus time profiles (Figure 3b), but a better illustration is given by the I_{ACE} intensities versus time (Figure 3c), which are not affected by the charging currents during the potential switch and, hence, truly represent the acetone formation rate with time. Moreover, given that a flow cell was used for these measurements, mass transport limitations

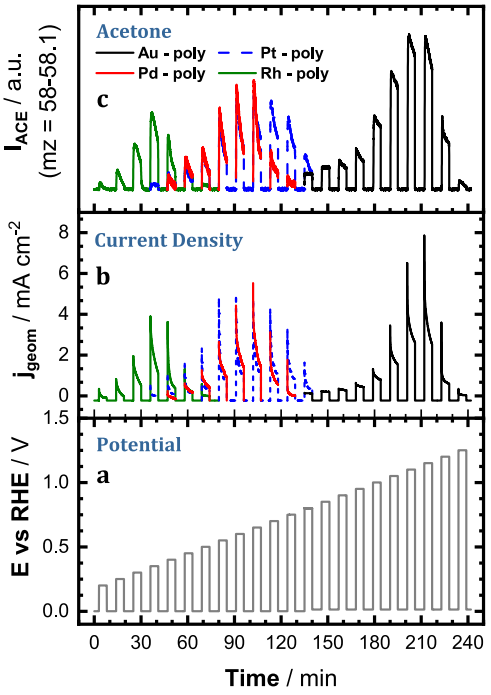

Figure 3. Chronoamperometric steps on Au, Pd, Pt, and Rh polycrystalline disk electrodes in a potential window from +0.2 to +1.25 V_{RHE} for 5 min, interrupted by steps at 0 V_{RHE} for 6 min, in 0.1 mol L^{-1} NaOH and 0.2 mol L^{-1} 2-propanol. The current densities and ion currents are shown for the aforementioned polycrystalline electrodes.

https://doi.org/10.1021/acscatal.3c03423
ACS Catal. 2023, 13, 14562−14569

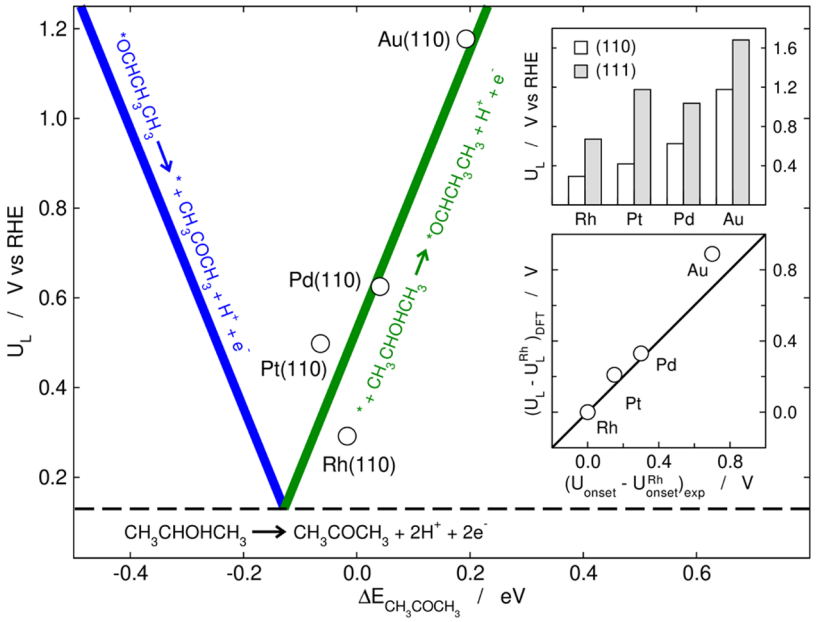

Figure 4. Computational modeling of 2-propanol oxidation to acetone. The limiting potentials on Rh, Pt, Pd, and Au are linearly related to the adsorption energies of acetone. The equations of the limiting steps are shown in each case. The dashed line corresponds to the equilibrium potential. Top inset: limiting potentials for the (110) and (111) facets of Rh, Pt, Pd, and Au. In all cases, the (110) facet provides lower limiting potentials. Bottom inset: parity plot comparing the experimental onset potentials and DFT-calculated limiting potentials using Rh as a reference.

are minimal and thus cannot be considered as a possible explanation for the rate decay. Although in a different environment, we previously showed increasing intensity of acetone-related bands with time by means of time-resolved infrared spectra, for Pt(111) and polycrystalline platinum in acid.[8] Other studies suggested that acetone does not adsorb on Pt(111), but did observe acetone adsorption on the other two basal planes, as well as minor formation of adsorbed CO on Pt(110).[9,39] In light of the above, and bearing in mind that these studies are focused on different systems (i.e., platinum surfaces in acid), the observed rate decay with time is attributed to catalyst deactivation, likely related to the gradual accumulation of acetone on the electrode surface, which has been evidenced for all four electrodes in alkaline media; see the spectra in Figure 2.

3.4. Computational Modeling. 2-Propanol oxidation to acetone ($CH_3CHOHCH_3 \rightarrow CH_3COCH_3 + 2H^+ + 2e^-$) was modeled as a two-step reaction with an oxygen-bound intermediate

$$* + CH_3CHOHCH_3 \rightarrow {}^*CH_3CHOCH_3 + H^+ + e^- \quad (1)$$

$$^*CH_3CHOCH_3 \rightarrow * + CH_3COCH_3 + H^+ + e^- \quad (2)$$

The pathway in eqs 1 and 2 can also be modeled in alkaline media by replacing eqs 1 and 2 by $*+ CH_3CHOCH_3^- \rightarrow {}^*CH_3CHOCH_3 + e^-$ and $^*CH_3CHOCH_3 + OH^- \rightarrow * + CH_3COCH_3 + H_2O + e^-$. While this would simply imply a shift in the energies related to the pK_a of 2-propanol, we have refrained from doing that here in view of the uncertainty in such pK_a, for which values in the range of 16−18 were found. We note that to make a one-to-one quantitative comparison to experiments in the lower inset of Figure 4, we referenced all data to Rh, which avoids the problem of having different reacting species compared to experiments. The adsorption configurations of $^*CH_3CHOCH_3$ and acetone on the (110) facets of the four metals under study are provided in Figure S4.

The polycrystalline disks used in our experiments contain numerous domains with various types of sites, such as terraces and undercoordinated defects. The voltammograms in Figure 1 contain the contributions to the overall activity of all those sites. Hence, to assert the nature of the active sites, we modeled the reaction on highly coordinated and undercoordinated sites. An example of the former are (111) terraces, and an example of the latter are the step edges of (110) slabs. As shown in the top inset of Figure 4, undercoordinated step edges provide for each metal lower limiting potentials (U_L). This can be rationalized by means of the Sabatier-type activity plot in the main panel of Figure 4: all metals are located on the weak-binding side where the reaction is limited by the first electrochemical step, namely, the formation of adsorbed isopropoxide ($^*CH_3CHOCH_3$). In other words, the four metals analyzed here are too noble in the sense that their binding to surface species is not strong enough. Because of this, undercoordination lowers the limiting potential until a thermodynamic minimum is reached.

According to Figure 4, the adsorption energy of acetone ($\Delta E_{CH_3COCH_3}$) can be used as a descriptor for the activity trends, and the minimum limiting potential is reached when such an adsorption energy is around −0.13 eV. Importantly, the adsorption energy of acetone can be readily computed with DFT and might as well be measured experimentally.

The activity order we obtain in terms of limiting potentials is Rh > Pt > Pd > Au, which coincides with the trend in experimental onset potentials extracted from Figure 1. In fact, if Rh(110) is used as a reference for the DFT data and polycrystalline Rh is used as a reference for the experimental data, the relative potentials agree well, as shown in the lower inset of Figure 4.

All in all, we observe with our computational model that the reaction intermediate of 2-propanol oxidation on late transition metals tends to be weakly bound such that the onset potential is enhanced by undercoordinated sites. Acetone tends to bind weakly to those metals, too, and its adsorption energy can be

https://doi.org/10.1021/acscatal.3c03423
ACS Catal. 2023, 13, 14562−14569

used as an activity descriptor. Because Rh, Pd, Pt, and Au are all located on the weak-binding side of the volcano, it is likely that less noble transition metals with stronger adsorption energies will be active for 2-propanol oxidation. The optimal activity should be found for sites that display adsorption energies of acetone of −0.13 eV, for which the volcano lines intersect the equilibrium potential line in Figure 4.

4. CONCLUSIONS

We studied the electrochemical oxidation of 2-propanol on noble metals in alkaline solution with experimental and computational methods and can draw the following conclusions:

- The activity, defined by the overpotential, decreases in the order Rh > Pt > Pd > Au. This is different from acidic electrolytes, where only platinum is active.
- The C−C bond does not break on any surface, leading to the selective formation of acetone.
- At high overpotentials, the reaction is limited by oxide formation.
- At a constant potential, gradual accumulation of acetone to the surface inhibits the reaction.
- The observed catalytic trends follow a simple correlation with the acetone adsorption energy: rhodium, which binds acetone more strongly exhibits the lowest overpotential, whereas Au, a weak-binding metal, exhibits the highest. This correlation could be extended in future works to include other transition metals.
- The most active sites of the reaction are located at undercoordinated defects on the four metal electrodes under study.

Overall, the fact that alkaline systems are not exclusively restricted to platinum-based electrodes opens the opportunity of looking into a broader range of materials that can act as efficient anodes for 2-propanol fuel cells.

■ ASSOCIATED CONTENT

Supporting Information

The Supporting Information is available free of charge at https://pubs.acs.org/doi/10.1021/acscatal.3c03423.

Linear sweep voltammograms for the four electrodes in alkaline and acidic conditions in the absence and presence of 2-propanol; EC-IRRAS spectra at various potentials for the four electrodes in *p*-polarization and *s*-polarization; and further details on the computational modeling, tabulated data, and coordinates of the simulated systems (PDF)

■ AUTHOR INFORMATION

Corresponding Authors

Iosif Mangoufis-Giasin − *Helmholtz-Institut Erlangen-Nürnberg for Renewable Energy (IEK-11), Forschungszentrum Jülich GmbH, 91058 Erlangen, Germany; Department of Chemical and Biological Engineering, Friedrich-Alexander-Universität Erlangen-Nürnberg, 91058 Erlangen, Germany*; Email: i.mangoufis@fz-juelich.de

Federico Calle-Vallejo − *Nano-Bio Spectroscopy Group and European Theoretical Spectroscopy Facility (ETSF), Department of Advanced Materials and Polymers: Physics, Chemistry and Technology, University of the Basque Country UPV/EHU, 20018 San Sebastián, Spain; IKERBASQUE, Basque Foundation for Science, 48009 Bilbao, Spain;* orcid.org/0000-0001-5147-8635; Email: federico.calle@ehu.es

Ioannis Katsounaros − *Helmholtz-Institut Erlangen-Nürnberg for Renewable Energy (IEK-11), Forschungszentrum Jülich GmbH, 91058 Erlangen, Germany;* orcid.org/0000-0001-6462-710X; Email: i.katsounaros@fz-juelich.de

Authors

Lukáš Fusek − *Interface Research and Catalysis, ECRC, Friedrich-Alexander-Universität Erlangen-Nürnberg, 91058 Erlangen, Germany; Faculty of Mathematics and Physics, Department of Surface and Plasma Science, Charles University, 18000 Prague, Czech Republic;* orcid.org/0000-0002-2189-4731

Tian Yang − *School of Physical Science and Technology, ShanghaiTech University, Shanghai 201210, People's Republic of China*

Peyman Khanipour − *Helmholtz-Institut Erlangen-Nürnberg for Renewable Energy (IEK-11), Forschungszentrum Jülich GmbH, 91058 Erlangen, Germany; Department of Chemical and Biological Engineering, Friedrich-Alexander-Universität Erlangen-Nürnberg, 91058 Erlangen, Germany*

Olaf Brummel − *Interface Research and Catalysis, ECRC, Friedrich-Alexander-Universität Erlangen-Nürnberg, 91058 Erlangen, Germany;* orcid.org/0000-0001-5968-0774

Jörg Libuda − *Interface Research and Catalysis, ECRC, Friedrich-Alexander-Universität Erlangen-Nürnberg, 91058 Erlangen, Germany;* orcid.org/0000-0003-4713-5941

Karl J. J. Mayrhofer − *Helmholtz-Institut Erlangen-Nürnberg for Renewable Energy (IEK-11), Forschungszentrum Jülich GmbH, 91058 Erlangen, Germany; Department of Chemical and Biological Engineering, Friedrich-Alexander-Universität Erlangen-Nürnberg, 91058 Erlangen, Germany;* orcid.org/0000-0002-4248-0431

Complete contact information is available at: https://pubs.acs.org/10.1021/acscatal.3c03423

Notes

The authors declare no competing financial interest.

■ ACKNOWLEDGMENTS

This work was funded by the Bavarian Ministry of Economic Affairs, Regional Development and Energy. The authors acknowledge additional financial support by the Deutsche Forschungsgemeinschaft (DFG) via Collaborative Research Centre SFB 1452—Catalysis at Liquid Interfaces (project431791331) and by the DFG via projects 322419553, 431733372, and 453560721 and by the German Federal Ministry of Education and Research (BMBF, Project Combined Infrared and X-ray Analytics of Energy Materials, CIXenergy 05K19WE1). L.F. thanks the Grant Agency of the Charles University (project GAUK 262120) for support. The authors acknowledge the support provided by the China Scholarship Council (CSC) during a visit of TY at the Friedrich-Alexander-Universität Erlangen-Nürnberg. This work also received financial support from grants PID2021-127957NB-I00 and TED2021-132550B−C21, which are funded by MCIN/AEI/10.13039/501100011033 and by the European Union. The use of supercomputing facilities at SURFsara was sponsored by NWO Physical Sciences, with financial support by NWO.

https://doi.org/10.1021/acscatal.3c03423
ACS Catal. 2023, 13, 14562−14569

REFERENCES

(1) Preuster, P.; Papp, C.; Wasserscheid, P. Liquid Organic Hydrogen Carriers (LOHCs): Toward a Hydrogen-Free Hydrogen Economy. *Acc. Chem. Res.* **2017**, *50* (1), 74−85.

(2) Sievi, G.; Geburtig, D.; Skeledzic, T.; Bösmann, A.; Preuster, P.; Brummel, O.; Waidhas, F.; Montero, M. A.; Khanipour, P.; Katsounaros, I.; Libuda, J.; Mayrhofer, K. J. J.; Wasserscheid, P. Towards an Efficient Liquid Organic Hydrogen Carrier Fuel Cell Concept. *Energy Environ. Sci.* **2019**, *12* (7), 2305−2314.

(3) Khanipour, P.; Speck, F. D.; Mangoufis-Giasin, I.; Mayrhofer, K. J. J.; Cherevko, S.; Katsounaros, I. Electrochemical Oxidation of Isopropanol on Platinum-Ruthenium Nanoparticles Studied with Real-Time Product and Dissolution Analytics. *ACS Appl. Mater. Interfaces* **2020**, *12* (30), 33670−33678.

(4) Gootzen, J. F. E.; Wonders, A. H.; Visscher, W.; Van Veen, J. A. R. Adsorption of C3 Alcohols, 1-Butanol, and Ethene on Platinized Platinum as Studied with FTIRS and DEMS. *Langmuir* **1997**, *13* (6), 1659−1667.

(5) Rodrigues, I. D. A.; De Souza, J. P. I.; Pastor, E.; Nart, F. C. Cleavage of the C-C Bond during the Electrooxidation of 1-Propanol and 2-Propanol: Effect of the Pt Morphology and of Codeposited Ru. *Langmuir* **1997**, *13* (25), 6829−6835.

(6) Gomes, J. F.; Oliveira, V. L.; Pratta, P. M. P.; Tremiliosi-Filho, G. Reactivity of Alcohols with Three-Carbon Atom Chain on Pt in Acidic Medium. *Electrocatalysis* **2015**, *6* (1), 7−19.

(7) Pastor, E.; González, S.; Arvia, A. J. Electroreactivity of Isopropanol on Platinum in Acids Studied by DEMS and FTIRS. *J. Electroanal. Chem.* **1995**, *395* (1−2), 233−242.

(8) Waidhas, F.; Haschke, S.; Khanipour, P.; Fromm, L.; Görling, A.; Bachmann, J.; Katsounaros, I.; Mayrhofer, K. J. J.; Brummel, O.; Libuda, J. Secondary Alcohols as Rechargeable Electrofuels: Electrooxidation of Isopropyl Alcohol at Pt Electrodes. *ACS Catal.* **2020**, *10* (12), 6831−6842.

(9) Mekazni, D. S.; Arán-Ais, R. M.; Herrero, E.; Feliu, J. M. On the Oxidation of Isopropanol on Platinum Single Crystal Electrodes. A Detailed Voltammetric and FTIR Study. *J. Power Sources* **2023**, *556* (September 2022), No. 232396.

(10) Mangoufis-Giasin, I.; Piqué, O.; Khanipour, P.; Mayrhofer, K. J. J.; Calle-Vallejo, F.; Katsounaros, I. Different Promoting Roles of Ruthenium for the Oxidation of Primary and Secondary Alcohols on PtRu Electrocatalysts. *J. Catal.* **2021**, *400*, 166−172.

(11) Yang, T.; Yang, J.; Deng, X.; Franz, E.; Fromm, L.; Taccardi, N.; Liu, Z.; Görling, A.; Wasserscheid, P.; Brummel, O.; Libuda, J. Modifying the Electrocatalytic Selectivity of Oxidation Reactions with Ionic Liquids. *Angew. Chem., Int. Ed.* **2022**, *61* (29), 1−5.

(12) Markiewicz, M. E. P.; Hebert, D. M.; Bergens, S. H. Electro-Oxidation of 2-Propanol on Platinum in Alkaline Electrolytes. *J. Power Sources* **2006**, *161* (2), 761−767.

(13) Cao, D.; Bergens, S. H. A Direct 2-Propanol Polymer Electrolyte Fuel Cell. *J. Power Sources* **2003**, *124* (1), 12−17.

(14) Liu, Y.; Zeng, Y.; Liu, R.; Wu, H.; Wang, G.; Cao, D. Poisoning of Acetone to Pt and Au Electrodes for Electrooxidation of 2-Propanol in Alkaline Medium. *Electrochim. Acta* **2012**, *76*, 174−178.

(15) Santasalo-Aarnio, A.; Kwon, Y.; Ahlberg, E.; Kontturi, K.; Kallio, T.; Koper, M. T. M. Comparison of Methanol, Ethanol and Iso-Propanol Oxidation on Pt and Pd Electrodes in Alkaline Media Studied by HPLC. *Electrochem. Commun.* **2011**, *13* (5), 466−469.

(16) Okanishi, T.; Katayama, Y.; Ito, R.; Muroyama, H.; Matsui, T.; Eguchi, K. Electrochemical Oxidation of 2-Propanol over Platinum and Palladium Electrodes in Alkaline Media Studied by in Situ Attenuated Total Reflection Infrared Spectroscopy. *Phys. Chem. Chem. Phys.* **2016**, *18* (15), 10109−10115.

(17) Ye, J.; Liu, J.; Xu, C.; Jiang, S. P.; Tong, Y. Electrooxidation of 2-Propanol on Pt, Pd and Au in Alkaline Medium. *Electrochem. Commun.* **2007**, *9* (12), 2760−2763.

(18) Choi, Y.; Sinev, I.; Mistry, H.; Zegkinoglou, I.; Roldan Cuenya, B. Probing the Dynamic Structure and Chemical State of Au Nanocatalysts during the Electrochemical Oxidation of 2-Propanol. *ACS Catal.* **2016**, *6* (5), 3396−3403.

(19) Xing, S.; Liu, Z.; Xue, Q.; Yin, S.; Li, F.; Cai, W.; Li, S.; Chen, P.; Jin, P.; Yao, H.; Chen, Y. Rh Nanoroses for Isopropanol Oxidation Reaction. *Appl. Catal., B* **2019**, *259* (July), No. 118082.

(20) Cheng, F.; Wang, H.; Sun, Z.; Ning, M.; Cai, Z.; Zhang, M. Electrodeposited Fabrication of Highly Ordered Pd Nanowire Arrays for Alcohol Electrooxidation. *Electrochem. Commun.* **2008**, *10* (5), 798−801.

(21) Serov, A.; Martinez, U.; Falase, A.; Atanassov, P. Highly Active Pd-Cu Catalysts for Electrooxidation of 2-Propanol. *Electrochem. Commun.* **2012**, *22* (1), 193−196.

(22) Zalineeva, A.; Serov, A.; Padilla, M.; Martinez, U.; Artyushkova, K.; Baranton, S.; Coutanceau, C.; Atanassov, P. Nano-Structured Pd-Sn Catalysts for Alcohol Electro-Oxidation in Alkaline Medium. *Electrochem. Commun.* **2015**, *57*, 48−51.

(23) Van Drunen, J.; Napporn, T. W.; Kokoh, B.; Jerkiewicz, G. Electrochemical Oxidation of Isopropanol Using a Nickel Foam Electrode. *J. Electroanal. Chem.* **2014**, *716*, 120−128.

(24) Khanipour, P.; Löffler, M.; Reichert, A. M.; Haase, F. T.; Mayrhofer, K. J. J.; Katsounaros, I. Electrochemical Real-Time Mass Spectrometry (EC-RTMS): Monitoring Electrochemical Reaction Products in Real Time. *Angew. Chem., Int. Ed.* **2019**, *58* (22), 7273−7277.

(25) Khanipour, P.; Haschke, S.; Bachmann, J.; Mayrhofer, K. J. J.; Katsounaros, I. Electrooxidation of Saturated C1-C3 Primary Alcohols on Platinum: Potential-Resolved Product Analysis with Electrochemical Real-Time Mass Spectrometry (EC-RTMS). *Electrochim. Acta* **2019**, *315*, 67−74.

(26) Faisal, F.; Bertram, M.; Stumm, C.; Waidhas, F.; Brummel, O.; Libuda, J. Preparation of Complex Model Electrocatalysts in Ultra-High Vacuum and Transfer into the Electrolyte for Electrochemical IR Spectroscopy and Other Techniques. *Rev. Sci. Instrum.* **2018**, *89* (11), No. 114101.

(27) Kresse, G.; Furthmüller, J. Efficient Iterative Schemes for Ab Initio Total-Energy Calculations Using a Plane-Wave Basis Set. *Phys. Rev. B* **1996**, *54* (16), 11169−11186.

(28) Perdew, J. P.; Burke, K.; Ernzerhof, M. Generalized Gradient Approximation Made Simple. *Phys. Rev. Lett.* **1996**, *77* (18), 3865−3868.

(29) Kresse, G.; Joubert, D. From Ultrasoft Pseudopotentials to the Projector Augmented-Wave Method. *Phys. Rev. B: Condens. Matter Mater. Phys.* **1999**, *59* (3), 1758−1775.

(30) Methfessel, M.; Paxton, A. T. High-Precision Sampling for Brillouin-Zone Integration in Metals. *Phys. Rev. B* **1989**, *40* (6), 3616−3621.

(31) Monkhorst, H. J.; Pack, J. D. Special Points for Brillouin-Zone Integrations. *Phys. Rev. B* **1976**, *13* (12), 5188−5192.

(32) Rendón-Calle, A.; Builes, S.; Calle-Vallejo, F. Applied Catalysis B : Environmental Substantial Improvement of Electrocatalytic Predictions by Systematic Assessment of Solvent Effects on Adsorption Energies. *Appl. Catal., B* **2020**, *276* (February), No. 119147.

(33) Romeo, E.; Illas, F.; Calle-Vallejo, F. Evaluating Adsorbate-Solvent Interactions: Are Dispersion Corrections Necessary? *J. Phys. Chem. C* **2023**, *127* (21), 10134−10139.

(34) Granda-Marulanda, L. P.; Rendón-Calle, A.; Builes, S.; Illas, F.; Koper, M. T. M.; Calle-Vallejo, F. A Semiempirical Method to Detect and Correct DFT-Based Gas-Phase Errors and Its Application in Electrocatalysis. *ACS Catal.* **2020**, *10* (12), 6900−6907.

(35) Urrego-Ortiz, R.; Builes, S.; Calle-Vallejo, F. Fast Correction of Errors in the DFT-Calculated Energies of Gaseous Nitrogen-Containing Species. *ChemCatChem* **2021**, *13* (10), 2508−2516.

(36) Calle-Vallejo, F.; Koper, M. T. M. Theoretical Considerations on the Electroreduction of CO to C_2 Species on Cu(100) Electrodes. *Angew. Chem.* **2013**, *125* (28), 7423−7426.

(37) Nørskov, J. K.; Rossmeisl, J.; Logadottir, A.; Lindqvist, L.; Kitchin, J. R.; Bligaard, T.; Jónsson, H. Origin of the Overpotential for Oxygen Reduction at a Fuel-Cell Cathode. *J. Phys. Chem. B* **2004**, *108* (46), 17886−17892.

https://doi.org/10.1021/acscatal.3c03423
ACS Catal. 2023, 13, 14562−14569

(38) Kwon, Y.; Lai, S. C. S.; Rodriguez, P.; Koper, M. T. M. Electrocatalytic Oxidation of Alcohols on Gold in Alkaline Media: Base or Gold Catalysis? *J. Am. Chem. Soc.* **2011**, *133* (18), 6914−6917.
(39) Mekazni, D. S.; Arán-Ais, R. M.; Feliu, J. M.; Herrero, E. Understanding the Electrochemical Hydrogenation of Acetone on Pt Single Crystal Electrodes. *J. Electroanal. Chem.* **2022**, *922* (August), No. 116697.
(40) Dellepiane, G.; Overend, J. Vibrational Spectra and Assignment of Acetone, Aαα Acetone-D3 and Acetone-D6. *Spectrochim. Acta* **1966**, *22* (4), 593−614.
(41) Iwasita, T.; Xia, X. Adsorption of Water at Pt(111) Electrode in HClO4 Solutions. the Potential of Zero Charge. *J. Electroanal. Chem.* **1996**, *411* (1−2), 95−102.
(42) Kunimatsu, K.; Shimazu, K.; Kita, H. Electrochemical Oxidation of CO on Pt in Acidic and Base Solutions. Part II. Structural Change of the Pt Surface and Mechanism of Electrooxidation of CO Studied by in-Situ Infrared Reflection Spectroscopy. *J. Electroanal. Chem.* **1988**, *256* (2), 371−385.
(43) Iwasita, T.; Nart, F. C. In Situ Infrared Spectroscopy at Electrochemical Interfaces. *Prog. Surf. Sci.* **1997**, *55* (4), 271−340.
(44) Faisal, F.; Bertram, M.; Stumm, C.; Wähler, T.; Schuster, R.; Lykhach, Y.; Neitzel, A.; Skála, T.; Tsud, N.; Beranová, K.; Prince, K. C.; Matolín, V.; Brummel, O.; Libuda, J. Electrocatalysis with Atomically Defined Model Systems: Metal-Support Interactions between Pt Nanoparticles and Co3O4(111) under Ultrahigh Vacuum and in Liquid Electrolytes. *J. Phys. Chem. C* **2018**, *122* (36), 20787−20799.
(45) Faisal, F.; Stumm, C.; Bertram, M.; Wähler, T.; Schuster, R.; Xiang, F.; Lytken, O.; Katsounaros, I.; Mayrhofer, K. J. J.; Schneider, M. A.; Brummel, O.; Libuda, J. Atomically-Defined Model Catalysts in Ultrahigh Vacuum and in Liquid Electrolytes: Particle Size-Dependent CO Adsorption on Pt Nanoparticles on Ordered Co3O4(111) Films. *Phys. Chem. Chem. Phys.* **2018**, *20* (36), 23702−23716.
(46) Sun, S. G.; Lin, Y. In Situ FTIR Spectroscopic Investigations of Reaction Mechanism of Isopropanol Oxidation on Platinum Single Crystal Electrodes. *Electrochim. Acta* **1996**, *41* (5 SPEC. ISS.), 693−700.
(47) Yang, T.; Kastenmeier, M.; Ronovský, M.; Fusek, L.; Skála, T.; Waidhas, F.; Bertram, M.; Tsud, N.; Matvija, P.; Prince, K. C.; Matolín, V.; Liu, Z.; Johánek, V.; Mysliveček, J.; Lykhach, Y.; Brummel, O.; Libuda, J. Selective Electrooxidation of 2-Propanol on Pt Nanoparticles Supported on Co3O4: An in-Situ Study on Atomically Defined Model Systems. *J. Phys. D: Appl. Phys.* **2021**, *54* (16), No. 164002.

https://doi.org/10.1021/acscatal.3c03423
ACS Catal. 2023, 13, 14562−14569